Applied Catalysis B: Environmental 254 (2019) 312–320

Contents lists available at ScienceDirect

Applied Catalysis B: Environmental

journal homepage: www.elsevier.com/locate/apcatb

From rice straw to magnetically recoverable nitrogen doped biochar: Efficient activation of peroxymonosulfate for the degradation of metolachlor

Chao Liu, Liwei Chen, Dahu Ding*, Tianming Cai*

College of Resources and Environmental Sciences, Nanjing Agricultural University, Nanjing 210095, China

ARTICLE INFO

Keywords:
Degradation
Sulfate radical
Singlet oxygen
Agricultural waste
LC-Q-TOF-MS

ABSTRACT

Conversion of agricultural biomass waste to value-added biochar based catalysts receives tremendous interests because it falls into the scope of resource recycle concept. In this work, a magnetic nitrogen doped biochar-supported $CoFe_2O_4$ composite (MNBC) was synthesized by using rice straw, an abundant agricultural waste as the precursor. The prepared catalyst exhibited excellent performance in catalytic degradation of metolachlor (MET), a broad-spectrum chloroacetanilide herbicide, by coupling with peroxymonosulfate (PMS). The pyrolysis temperature played a significant role in the activity of the resultant catalysts. Among others, $MNBC_{800}$ catalyst performed the best stability and reusability. In-situ (EPR) analysis revealed that $SO_4^{\bullet-}$, •OH and $^1O_2$ participated into the degradation process and the $SO_4^{\bullet-}$ was the major contributor. The degradation was promoted at neutral and weak basic conditions, whilst significantly inhibited at strong basic condition (pH = 11). Eleven degradation intermediates were successfully identified through liquid chromatography – quadrupole time-of-flight – mass spectrometer (LC-Q-TOF-MS). The degradation mainly occurred via hydroxylation, dechlorination, and dealkylation reactions. Additionally, though the degradation was greatly inhibited in real wastewater, it was not remarkably influenced in river and groundwater, implying its applicability in river/groundwater remediation. Eventually, the easy separation and low toxicity make the catalyst promising for the degradation of MET from several aquatic systems. This study would pave the way to the catalytic degradations of organic pollutants by low-cost biochar based catalysts.

1. Introduction

Huge amount of agricultural waste is discarded associated with agricultural production each year. Statistically, the total amount of agricultural wastes produced in 2013 was 1.75×10^9 tons in China, of which crop straw was 9.93×10^8 tons (accounting for 56.8%) [1]. The safe disposal and utilization of the carbon-rich biomass residue is a big challenge.

The traditional method (e.g. incineration) not only fails to effectively recycle the resource, but also leads to the severe atmospheric pollution (emission of greenhouse gases). For instance, the direct burning of the crop straw in countryside is now strictly prohibited in China. Alternatively, the green and clean technologies (e.g. composting, anaerobic digestion, *etc.*) can convert the agricultural wastes into value-added organic fertilizer and bioenergy (biofuel and biogas), holding great promise for "win-win" strategy. Among them, the conversion of carbon-rich biomass to the value-added biochar is an attractive option.

Biochar is prepared through thermal decomposition of a wide range of waste biomass under the temperatures below 700 °C and oxygen-limited conditions [2]. It is low-cost, widely available, and environmentally friendly. According to its tunable specific surface area (SSA) and abundant surface functional groups, biochar has shown great potentials in soil amendments and contaminants abatement [3,4]. For example, biochar can improve the ion exchange capacity, porosity, water holding capacity, retention of nutrients or microbial activity of the soil [5]. Moreover, biochar displays high affinity to both organic and inorganic contaminants [6]. Compared with its applications in soil amendment and adsorption of contaminants, its role in the catalytic oxidation of refractory organic pollutants is rarely explored. Fang et al. [7] reported that the persistent free radicals (PFRs) on biochar, generated from incomplete thermal decomposition was the redox centers to decompose H_2O_2 to hydroxyl radicals (•OH). Similar to H_2O_2, the persulfates (including peroxymonosulfate (PMS) and peroxydisulfate (PDS)) also contain O—O bond, which is supposed to be cleaved by the PFRs on biochar. The resulted sulfate radical ($SO_4^{\bullet-}$) possesses a comparative redox potential (2.5–3.1 V) and better selectivity towards organics with unsaturated bond and aromatic structure than •OH [8]. Therefore, it is hypothesized that the PMS can be catalyzed by biochar

* Corresponding authors at: 1 Weigang, Xuanwu District, Nanjing, 210095, China.
E-mail addresses: ddh@njau.edu.cn (D. Ding), ctm@njau.edu.cn (T. Cai).

https://doi.org/10.1016/j.apcatb.2019.05.014
Received 24 December 2018; Received in revised form 21 April 2019; Accepted 2 May 2019
Available online 03 May 2019
0926-3373/

to generate sulfate radicals. Furthermore, the catalytic activity of biochar could be enhanced by substitutional doping with adventitious nitrogen atoms [9]. The doped nitrogen can not only increase the surface basicity which is favorable for PMS adsorption, but also facilitate electron transfer reaction with PMS by activating the neighboring sp^2 carbon atoms [10,11]. More recently, our group found that the biochar modification could significantly promote the activity of Co_3O_4 due to the alteration of the surface chemical compositions [12].

Despite of the inspiring progress, the application of biochar in the water treatment still suffers from the inconvenient separation. To this end, magnetic biochar is synthesized by using Fe_3O_4 as the additive [13,14]. Noteworthily, the active Fe^{2+} of Fe_3O_4 could also activate PDS/PMS to produce sulfate radicals [15,16]. However, its reactivity is unsatisfactory when comparing with other transition metals, such as Co^{2+} [17]. Alternatively, cobalt ferrite (CF, with a typical formula $CoFe_2O_4$) is another ideal magnetic mixed metal oxide [18]. More importantly, the active cobalt species (Co^{2+}) exhibit much better reactivity than Fe^{2+} towards the decomposition of peroxymonosulfate (PMS) [17]. By depositing CF nanoparticles on the 2-dimensional graphene oxide (GO), the magnetic $CoFe_2O_4$-GO composite was synthesized by our group [19]. However, the field applications of the graphene based nanomaterials are strictly limited by the high preparation cost at the current stage.

Herein, we report a novel magnetic nitrogen doped biochar (MNBC) by using rice straw as the feedstock of biochar due to its abundance in agricultural wastes. For the first time, its catalytic behavior towards the decomposition of PMS was investigated in terms of the degradation of metolachlor (MET), a broad-spectrum chloroacetanilide herbicide. The effect of pyrolysis temperature on the intrinsic (*e.g.* surface chemistry, degree of graphitization, *etc.*) and extrinsic (*e.g.* specific surface area, catalytic activity, *etc.*) properties of the catalysts were systematically investigated. The degradation behavior in three successive cycles were comparatively studied. The reactive oxidative species and degradation products were identified, respectively. Accordingly, the probable degradation pathway was established. Additionally, the toxicity of the degradation products towards green alga Chlorella sp. was tentatively evaluated.

2. Materials and methods

2.1. Chemical and reagents

Metolachlor (98%), potassium monopersulfate triple salt ($KHSO_5{\cdot}0.5KHSO_4{\cdot}0.5K_2SO_4$, ≥47% $KHSO_5$ basis), 5,5-Dimethyl-1-pyrroline N-oxide (DMPO, 97%), and 2,2,6,6-tetramethyl-4-piperidinol (TEMP, > 98%) were purchased from Aladdin, China. All the other chemicals were at least of analytic grade and used without further purification. Deionized water was produced through a water purification system (EPED-10TF).

2.2. Preparation and characterizations of biochar based catalysts

Rice straw is collected from a local farmland in Jiangsu, China, washed and naturally air dried. The dried rice straw is then mechanically grinded by using a stainless grinding machine and sieved to < 2.0 mm particles. The resulted rice straw powder is stored in a ziplock bag and used as the feedstock of biochar.

The magnetic nitrogen doped biochar catalysts were prepared through a robust impregnation-pyrolysis process. Typically, 2.91 g Co $(NO_3)_2{\cdot}6H_2O$ and 5.56 g $FeSO_4{\cdot}7H_2O$ were firstly dissolved into 80 mL water. Urea (3.0 g) and ascorbic acid (2.5 g) were added into the above mixture to serve as the nitrogen source and reductant, respectively. After that, 3 g rice straw was thoroughly impregnated into the mixture and the water content was evaporated at 80 °C in an oven. The cobalt and iron salts impregnated rice straw was transferred into a ceramic crucible and covered with a lid to supply an oxygen-limited condition. The crucible was finally heated to a desired temperature (400–800 °C) in a muffle furnace with a ramp of 5 °C/min and maintained for 4 h. After cooling to room temperature, the biochar samples were washed with water for several times to remove the impurities and residual metal species. The prepared catalysts were designated as MNBCx, where x represents pyrolysis temperature (400, 500, 600, 700, and 800 °C). Meanwhile, the unmodified biochar sample was prepared by directly thermal conversion of rice straw at pyrolysis temperature of 800 °C and designated to be BC_{800}. The $CoFe_2O_4$ nanoparticles were hydrothermally prepared according to our previous work and then calcined at 800 °C for 4 h [18]. Nitrogen doped biochar (NBC) samples were prepared through the same carbonization process with rice straw and urea as the precursor.

The prepared MNBC catalysts were characterized with SEM, Raman, XRD, XPS, and N_2 adsorption/desorption apparatus, respectively. The detailed information was provided in the Supporting Information Text S1.

2.3. Catalytic degradation of MET

The catalytic degradation experiments were carried out in conical flasks (100 mL) placed on a rotary shaker at room temperature (25 ± 1 °C). Prior to the catalytic reaction, a certain amount of solid catalyst was dispersed into 50 mL of 10 mg L^{-1} MET solution. The solution pH was adjusted with 0.1 M H_2SO_4 or NaOH if necessary but not buffered. The mixture was rotated for 30 min to establish the adsorption-desorption equilibrium. Afterwards, an aliquot PMS stock solution (200 mM) was injected into the solution to initiate the reaction. At regular time intervals, 1.5 mL liquid sample was collected, filtered through a 0.22 μm filter film, and detected for MET concentration immediately. To evaluate the stability of the prepared catalyst, the catalyst was collected after a degradation cycle, washed with water and used in the next catalytic reaction. The degradation performances in the three successive cycles were recorded.

To identify the reactive oxidative species in the degradation process and distinguish their contributions, *in-situ* electron paramagnetic resonance (EPR) analysis and radical scavenging assays were conducted, respectively. To evaluate the degradation of MET in different aquatic systems, the river water (collected from the Yangtze River in Nanjing), groundwater (collected from the Fujian province), and biologically treated wastewater (collected from a local agrochemical plant in Jiangsu province) were used as the background solutions (spiked with 10 mg L^{-1} MET), respectively. The collected water samples were filtered with qualitative filter paper (Whatman, GE) upon arrival and stored at 4 °C prior to the use (within 2 months). The basic information of the water samples were summarized in Supporting Information Table S1.

All the experiments were conducted in at least duplicate and the results were expressed as mean values ± standard deviations.

2.4. Kinetic modelling study

Pseudo-first order kinetic model was used to mimic the degradation kinetics of MET in this study. Degradation data in the initial 10 min were adopted for the kinetic modeling. The following equation was utilized to calculate the apparent rate constant k_{app}.

$$\ln\left(\frac{C_t}{C_0}\right) = -k_{app}t \quad (1)$$

where $C_0$is initial concentration of MET, $C_t$is concentration of MET at time t, $k_{app}$is the apparent pseudo-first order constant. By plotting ln (C_t/C_0) versus t, k_{app}can be graphically calculated.

2.5. Analytical methods

Residual MET in the liquid phase was detected on a high performance liquid chromatograph (FL 5090) equipped with a UV detector (detection wavelength was 230 nm) and a C18 reversed-phase column. The mobile phase was consisted of water and methanol (150 mL: 850 mL), in which 0.2 mL formic acid was added. The flow rate was 1.0 mL min^{-1} and the injection volume was 20 μL. Identification of the transformation products of MET was carried out using a liquid chromatography – quadrupole time-of-flight – mass spectrometer (LC-Q-TOF-MS). The detailed procedure was provided in Supporting Information Text S2.

The leachable iron and cobalt ions were measured by inductively coupled plasma (Varian 720). Total organic carbon (TOC, mg C L^{-1}) was determined using a Shimadzu 5000A TOC analyzer (Shimadzu, Japan). The concentrations of Cl- was measured with ion chromatography (ICS-900, DIONEX) equipped with a DS5 conductivity detector and Dionex IonPac® AS23 column (4 × 250 mm). The concentration of NH_4^+ was analyzed according to the Nessler's reagent colorimetric method. Solution pH was detected by using a PHS-3C pH meter (INESA) equipped with an E-201-C electrode. The operation details of the EPR analysis were provided in Supporting Information Text S3.

2.6. Toxicity evaluation

The toxicity of the degradation products to aquatic organisms was investigated by using green algae Chlorella sp. obtained from the Institute of Oceanology, Chinese Academy of Sciences, Qingdao. The detailed protocol for the preparation of the cultivation medium could be found elsewhere [20]. The growth rate was monitored in terms of the optical density (OD) at wavelength of 680 nm. Additionally, the concentrations of Chlorophyll A and Chlorophyll B was measured with microplate reader (SpectraMax M5) at wavelength of 666 and 653 nm, respectively. Notably, the initial culture OD was adjusted to $OD_{680\ nm} = 0.2$ prior to the toxicity experiment. The detailed analytic methods were given in Supporting Information Text S4.

3. Results and discussion

3.1. Characterizations

The XRD patterns (Fig. 1A) of the prepared MNBC catalysts clearly demonstrated the formation of $CoFe_2O_4$ crystals because the peaks matched well with cubic spinel phase of $CoFe_2O_4$ (JCPDS PDF#22-1086) [18]. With the increase of the pyrolysis temperature, the diffraction intensity increased, suggesting a higher crystallization degree. Two broadened peaks centered at around 25° and 44° were found in the prepared BC_{800} sample, corresponding to the (002) and (101) reflections of graphite respectively. However, these two peaks disappeared in the MNBC samples probably due to that they were overlapped by the strong $CoFe_2O_4$ diffraction peaks.

Nitrogen adsorption/desorption isotherms (Fig. 1B) and specific surface area (S_{BET}) result (Table 1) illustrated that the MNBC catalysts prepared at higher temperature exhibited a higher specific surface area. The "jumping" improvement of S_{BET} for the MNBC prepared at a high pyrolysis temperature (> 700 °C) was probably due to the volatilization of tar compounds to create a richer porous structure [21]. The S_{BET} value of $MNBC_{800}$ was much higher than that of $CoFe_2O_4$ nanoparticles (1.3 $m^2 g^{-1}$ as provided in Fig. S1) and even higher than previously reported $CoFe_2O_4$-graphene oxide composite (43.9 $m^2 g^{-1}$) [19]. However, it was much lower when comparing with BC_{800} sample, suggesting that the loaded $CoFe_2O_4$ nanoparticles greatly covered the surface (from 516.2 $m^2 g^{-1}$ to 150.7 $m^2 g^{-1}$) and blocking the pores (from 0.255 $cm^3 g^{-1}$ to 0.081 $cm^3 g^{-1}$) of the biochar substrate. To verify this deduction, the morphological observation was conducted and the SEM images (Fig. S2) clearly demonstrated that the $CoFe_2O_4$ nanoparticles were regularly distributed on the surface and blocked the pores of the biochar substrate.

Moreover, Raman spectra exhibited two characteristic bands located at ~1340 cm^{-1} and ~1590 cm^{-1}, corresponding to the D band and G band of carbon materials (Fig. S3). Specifically, the D band corresponded to disordered carbon or defective graphitic structures, whilst the G band was associated with E_{2g} mode vibration of the intact honeycomb-like sp^2 hybridized carbon network. Therefore, the defective degree of carbon materials could be identified through the intensity ratio of I_D/I_G [22]. As indicated in Table 1, the I_D/I_G value increased with the pyrolysis temperature (< 600 °C), suggesting more defects

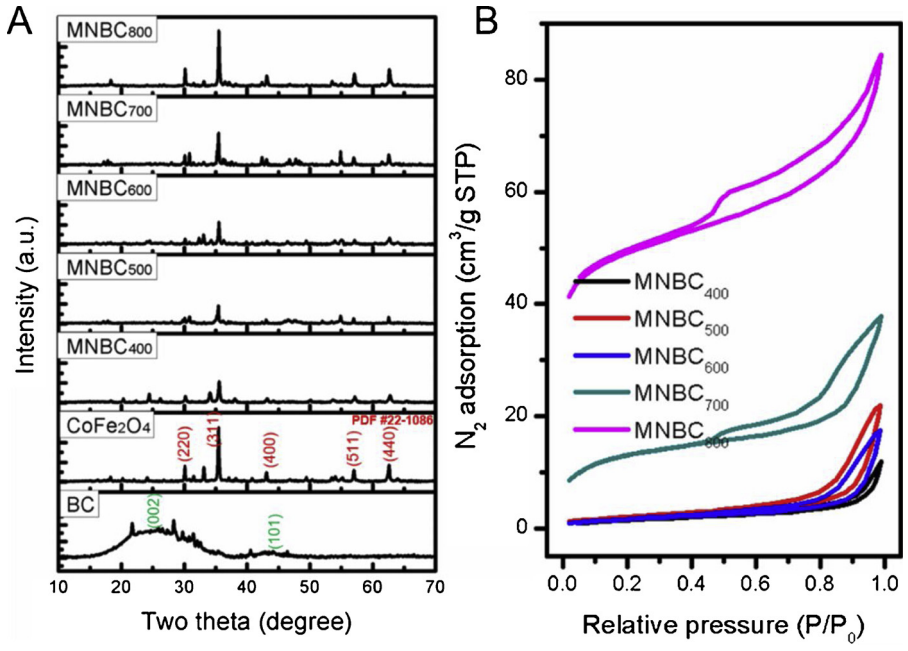

Fig. 1. XRD patterns (A) and N_2 adsorption/desorption isotherms (B) of the prepared catalysts.

Table 1
Properties of the catalysts.

Catalyst	C[a]	N[a]	N/C	O[a]	O/C	Graphitic N (%)	S_{BET} (m^2 g^{-1})	Pore volume (cm^3/g)	I_D/I_G[b]	k_{app} ($\times 10^{-2}$ min^{-1}) [c]
$MNBC_{400}$	35.6	9.43	0.26	46.8	1.31	24.1	5.3	0.020	0.97	4.54
$MNBC_{500}$	66.1	8.46	0.13	19.7	0.30	21.9	7.1	0.035	1.06	4.65
$MNBC_{600}$	59.1	7.43	0.12	29.3	0.49	27.0	6.0	0.029	1.13	4.93
$MNBC_{700}$	56.3	3.97	0.07	36.4	0.65	31.7	42.5	0.055	1.03	7.11
$MNBC_{800}$	76.4	1.53	0.02	20.2	0.26	60.8	150.7	0.081	0.79	10.4

[a] Obtained from the XPS results.
[b] Calculated from the Raman spectra.
[c] Experimental conditions: [MET] = 10 mg L^{-1}, [Catalyst] = 200 mg L^{-1}, [PMS] = 0.5 mM, [Reaction time] = 40 min, pH unadjusted.

formed during the thermolysis [9]. However, the I_D/I_G value significantly decreased when the temperature was 800 °C, indicating a high graphitization degree obtained. It was suggested that the graphitic structure was conductive to the charge transfer process and a high graphitization degree was helpful for promoting electron transfer between PMS and carbon catalysts, thus boosting the non-radical degradation pathway [23].

The wide survey XPS spectra (Fig. S4) confirmed the presence of C (284.5 eV), O (532.5 eV), N (400.0 eV), Co, and Fe in the prepared MNBC catalysts. It was clear that the MNBC catalysts prepared at 500–800 °C were carbon-rich. The O/C atomic ratios as the indication of polar-group content roughly decreased with the increase of the pyrolysis temperature (from 1.31 to 0.26), respectively. The N/C atomic ratios drastically decreased due to the nitrogen evaporation (from 0.26 to 0.02). Moreover, the N 1s XPS spectra could be deconvoluted into three components, which were pyridinic N (N in 6-member ring, centered at 398.4 ± 0.2 eV), pyrrolic N (N in 5-member ring, centered at 399.8 ± 0.2 eV) and graphitic N (N in graphitic carbon plane, centered at 400.7 ± 0.4 eV) [24,25]. With the increase of pyrolysis temperature, an obvious upshift of the binding energy was observed (Fig. S5). Moreover, as evidenced in Table 1, the proportion of graphitic N increased with the pyrolysis temperature (from 24.1%–60.8%). This was because that graphitic N was more thermally stable than pyridinic N and pyrrolic N and the latter nitrogen species were transformed to graphitic N during the thermal treatment [26]. It was suggested that the graphitic N was more reactive in catalytic reactions such as oxygen-reduction reactions [27] and persulfate activation [28] than the other nitrogen species.

Besides nitrogen, the oxygen-containing functional groups also played an important role in the catalytic reactions. As depicted in Fig. S6, the high resolution XPS O 1s spectra could also be resolved to three components, which were ascribed to O—C in the biochar (532 ± 0.4 eV), the O-Co in $CoFe_2O_4$ interfacial bonding structure (531 ± 0.2 eV), and the lattice oxygen (530 ± 0.2 eV) in MFe_2O_4, respectively [29]. All the spectra indicated that the dominant oxygen species were O—C and O-Co.

Fig. S7 showed that the XPS C1 s envelops were centered at 284.5 ± 0.2 eV with a tail at higher binding energies, indicating the existence of carbon atoms connected to N and O heteroatoms [30]. The C1 s peaks were fitted to five components at around 284.4, 285.6, 286.5, and 287.8 eV, corresponding to C—C/C=C in aromatic rings, C—OH and C=N, epoxy C—O—C, C=O and C—N, respectively. No significant change was observed in the different catalysts.

3.2. Catalytic degradation performance

As illustrated in Fig. S8, the degradation of MET by PMS was insignificant. No more than 10% was eliminated from the aqueous solution within 40 min, indicating PMS could not oxidize MET without external activation. After coupling with MNBC catalysts, a distinct synergistic effect was observed and the MET was rapidly degraded (Fig. S9). The kinetic rate constants of the catalysts followed: $MNBC_{800}$ > $MNBC_{700}$ > $MNBC_{600}$ ≈ $MNBC_{500}$ ≈ $MNBC_{400}$ (Table 1). Moreover, $MNBC_{800}$ exhibited better catalytic activity than bare $CoFe_2O_4$, revealing the important role of biochar. On one hand, the biochar could serve as a substrate to avoid the aggregation of magnetic $CoFe_2O_4$ nanoparticles. On the other hand, the N-doped biochar itself could effectively activate PMS via radical/non-radical pathways (Fig. S10) [9]. By plotting ln(k_{app}) versus ln(S_{BET}), a good linearity was developed (R^2 = 0.984) (Fig. S11), suggesting the beneficial role of surface area in the heterogeneous activation process. It was well accepted that the exposed surface was beneficial for the interaction between catalyst and PMS and thus accelerated the generation of sulfate radicals. Similarly, a nitrogen doped biochar catalyst prepared at 900 °C showed the best catalytic activity than those prepared at 400 °C, 700 °C, and 800 °C due to its highest S_{BET} (from 71.5 to 496.7 $m^2 g^{-1}$) [9]. Additionally, the TOC reduction process was rather time-consuming and $MNBC_{800}$ displayed the best performance (38.8% within 360 min, Fig. S12). Likewise, in an electro-Fenton process, the MET could be totally eliminated within 90 min while the TOC only declined from 50 mg L^{-1} to around 40 mg L^{-1} [31]. The incomplete mineralization might imply the generation and accumulation of refractory degradation intermediates [32]. The degradation intermediates might pose higher toxicity than their parent compound and thus deserve to be further characterized, which will be discussed in the following sections.

The poor reusability performance was usually reported for the metal-free catalysts [26,33]. A plausible reason was that the metal-free carbon based catalysts relied on its adsorption capacity towards PMS in the degradation process. Once the surface site was occupied with degradation products/intermediates, the interaction between PMS and catalyst was greatly depressed. As a result, the stability of the metal-free carbon catalysts were usually not comparable to those of metal oxides [34]. However, the adsorption results clearly indicated that the adsorption affinity of $MNBC_{800}$ towards MET was remarkably decreased compared with that of BC_{800} (Fig. S13). Consequently, by magnetic modification with $CoFe_2O_4$, the reusability of prepared MNBC catalysts, especially $MNBC_{800}$ showed advantages than other reported carbon based catalysts. For instance, the bisphenol A removal efficiency significantly decreased from 99% to 52% and 25% in the three consecutive cycles by using nitrogen doped biochar catalyzed PMS process [35]. Nevertheless, though the k_{app} gradually decreased, a relatively high removal efficiency (> 80%) could be maintained by using $MNBC_{800}$/PMS process in the three successive cycles (Fig. 2). This promising result might imply the operation cost could be greatly reduced during the field applications.

For cobalt-based catalysts, the secondary pollution issue caused by the released cobalt ions was of great concern. As a heavy metal, cobalt ions released into ecosystems were possibly toxic and carcinogenic, leading to serious health problems such as asthma, pneumonia and cardiomyopathy [36,37]. Apart from this, the loss of active metal ions might also lead to the significant deterioration of the catalytic performance. By using graphene oxide as the substrate, the strong Co—OH bond was expected and the active Co^{2+} was stabilized [19,38]. In this study, as evidenced in Fig. S14, no more than 0.3 mg L^{-1} Co^{2+} was detected after the degradation reaction, revealing the high stability of the prepared MNBC catalysts. In contrast, more than 0.5 mg L^{-1} was

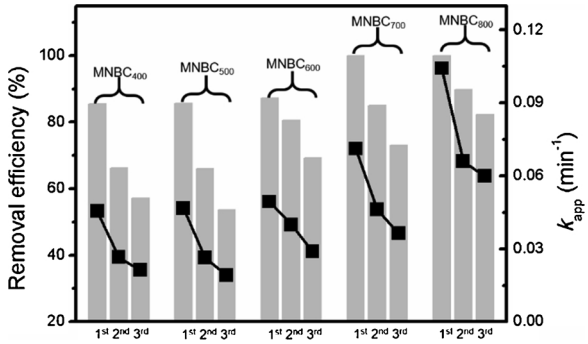

Fig. 2. Degradation profiles during three successive catalytic degradation runs. (Experimental conditions: [MET] = 10 mg L^{-1}, [Catalyst] = 200 mg L^{-1}, [PMS] = 0.5 mM, [Reaction time] = 40 min, pH unadjusted, columns represent the removal efficiency, scatters represent the k_{app}).

released by using $CoFe_2O_4$ as the catalyst. The extremely low released Co^{2+} was probably attributable to the following two reasons. Firstly, the cobalt species formed Co-O-C bonds with biochar substrate. Besides, Co/Fe-N_x bond might be occurred in the presence of Co/Fe metal and nitrogen species, preventing their loss [39]. Additionally, the extremely low leachable metal ions also excluded the homogeneous activation process.

Effect of solution pH on the degradation process was examined (Fig. 3). Consistent with previous studies, the near-neutral conditions were found to be favorable for the degradation in contrast to excessively acidic or alkaline conditions [8,40]. Nevertheless, when the pH was decreased to 3, approximately 24.1% of MET was degraded within 40 min. Moreover, a significant deterioration of the degradation was observed when the pH was 11. At acidic condition, the H_2SO_5 would become the main species instead of HSO_5^- because its second acid dissociation constant was 9.4 [41]. Consequently, the generation of $SO_4^{\bullet-}$ was obstructed. At basic condition, PMS species unlikely interact with the negatively charged surface of catalysts due to the electrostatic repulsion effect, hindering the generation of $SO_4^{\bullet-}$ [42]. When the pH was above 10, cobalt hydroxide complexes would be greatly produced, leading to the decreased oxidation potential and catalytic activity [43]. Additionally, the base catalyzed hydrolysis of PMS to sulfate anion and hydrogen peroxide would be expected at basic conditions (Eqs. (2)–(5)).

$$HSO_5^- \rightarrow SO_5^{2-} + H^+,\ pKa = 9.4 \quad (2)$$

$$HSO_5^- + H_2O \rightarrow HSO_4^- + H_2O_2 \quad (3)$$

$$SO_5^{2-} + H_2O \rightarrow SO_4^{2-} + H_2O_2 \quad (4)$$

$$HSO_5^- + 2OH^- \rightarrow 2SO_4^{2-} + H_2O + O_2 \quad (5)$$

The PMS dose was proportional to the pseudo-first-kinetic constant k_{app} with a linear relationship ($k_{app} = 0.126 \times [PMS] + 0.028$). Specifically, at the same catalyst dose condition, the degradation rate of MET rise with the PMS dose, the k_{app} was 0.023, 0.0442, 0.1043, 0.1818, and 0.3957 min^{-1} corresponding to the PMS dose of 0.1, 0.25, 0.5, 1.0 and 3.0 mM, respectively. This was quite expectable because radical species came from the decomposition of PMS [44].

3.3. Catalytic mechanism

For metal based catalytic reactions, the radical species (i.e. $SO_4^{\bullet-}$ and •OH) usually dominated the degradation process [8,44]. In contrast, singlet oxygen ($^1O_2$) and non-radical pathways emerged in metal-free carbonaceous catalyst activated PMS processes [45]. Therefore, the involvements of $SO_4^{\bullet-}$, •OH, and $^1O_2$ were anticipated in the $MNBC_{800}$/PMS process.

To confirm the speculation, the in-situ EPR analysis were conducted by adopting DMPO and TEMP as the radical spin trapping agents. As shown in Fig. 4, with assistance of DMPO, the typical seven-line EPR signal attributed to DMPOX spin-adduct rather than DMPO-SO_4 and DMPO-OH signals was immediately identified in the initial 2 min [46,47]. Then, the signal was gradually converted to DMPO-SO_4 (with hyperfine coupling constants of $\alpha_H = 1.44$ G, $\alpha_H = 0.76$ G, $\alpha_N = 15.02$ G, and $\alpha_H = 14.81$ G) and finally DMPO-OH (with hyperfine coupling constants of $\alpha_N = 15.05$ G and $\alpha_H = 14.21$ G) peaks. The initially occurred DMPOX signals should be attributed to the strongly oxidative ability through the interaction between $MNBC_{800}$ and PMS [23,48]. Additionally, the $^1O_2$ could also directly oxidize DMPO into DMPOX with a rate constant of approximately 1.8×10^7 M^{-1} s^{-1} [49]. The finally occurred DMPO-OH signal was probably ascribed to that the DMPO-SO_4 might react undesirably with H_2O via nucleophilic substitution reaction to yield DMPO-OH at a considerably fast reaction rate (e.g. $t_{1/2}$ of DMPO-SO_4 = 95 s in water) [33]. These results clearly confirmed the participation of free radicals in the catalytic reaction. Moreover, by using TEMP (the spin trapping agent for $^1O_2$) as the spin trapping agent, a representative triplet EPR spectrum (1:1:1, $\alpha = 17.2$ G) appeared, corresponding to the oxidized TEMP by $^1O_2$ [50]. The intensity increased sharply in the initial 10 min, implying that continuous generation of $^1O_2$. After 10 min, the intensity decreased probably due to the consuming of $^1O_2$ by MET.

To further distinguish their contributions, the chemical scavengers, methanol (MeOH) for both $SO_4^{\bullet-}$ and •OH, *tert*-butanol (TBA) for •OH,

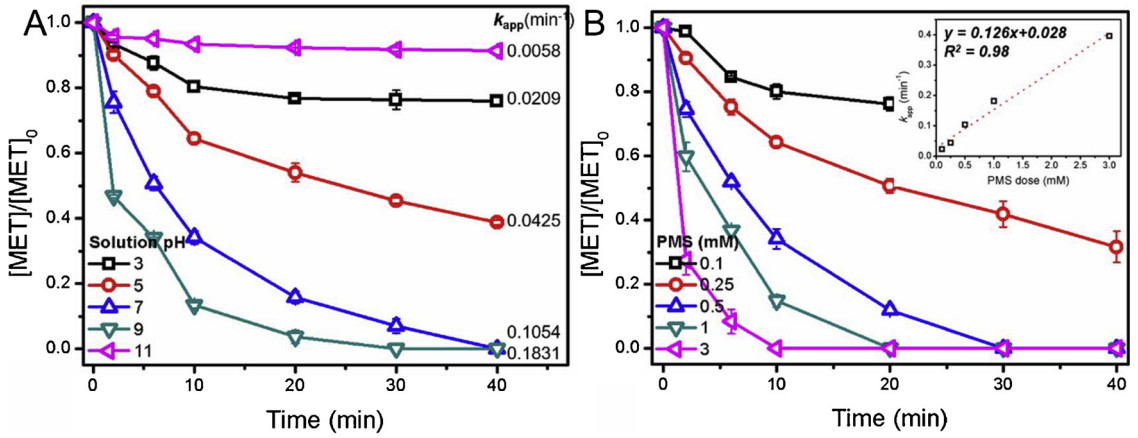

Fig. 3. Effects of solution pH (A) and PMS concentration (B) on the MET degradation process. (Experimental conditions: [MET] = 10 mg L^{-1}, [$MNBC_{800}$] = 200 mg L^{-1}, [PMS] = 0.5 mM in Panel A, pH unadjusted in Panel B, the inset of Panel B shows the linear relationship between PMS dose and derived k_{app}).

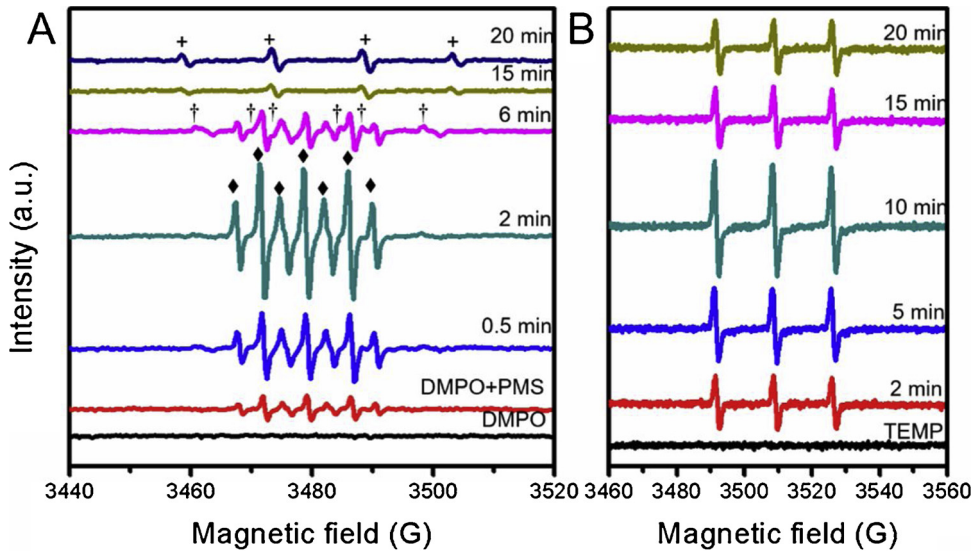

Fig. 4. Detected EPR signals by using DMPO (A) and TEMP (B) as the spin trapping agents. (♦ represents the DMPOX EPR signal, † represents the DMPO-SO_4 EPR signal, + represents the DMPO-OH EPR signal).

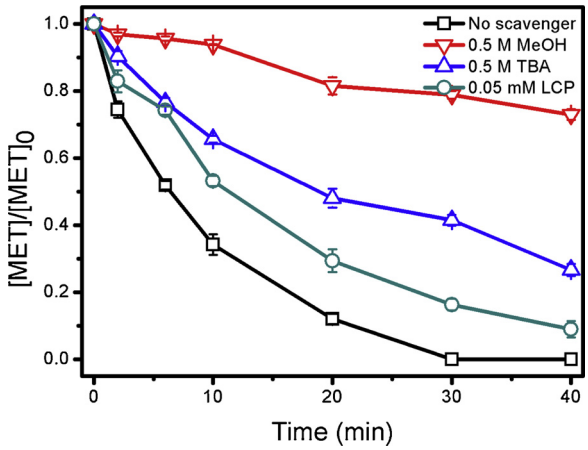

Fig. 5. Effect of radical quenching agents on the degradation process. (Experimental conditions: [MET] = 10 mg L^{-1}, [$MNBC_{800}$] = 200 mg L^{-1}, [PMS] = 0.5 mM, [MeOH] = [TBA] = 0.5 M, [LCP] = 0.05 mM, pH unadjusted).

lycopene (LCP) for $^1O_2$ were introduced into the reaction mixture respectively. As shown in Fig. 5, TBA and LCP could moderately inhibit the MET degradation while MeOH brought a detrimental effect on the degradation, revealing the major role of $SO_4^{\bullet-}$ in the degradation process.

Based on the above discussion, the catalytic mechanism could be depicted in Scheme 1. Generally speaking, two pathways (i.e. radical and non-radical pathways) took place in the degradation process. On the surface of $CoFe_2O_4$ nanoparticles, the sulfate radicals were produced through the redox reactions between Co^{2+} and PMS (Eqs. (6) and (7)) [51]. On the surface of nitrogen doped biochar, both routine radical [52,53] and novel non-radical [54–56] pathways were previously reported. The hydroxyl groups on the surface of biochar might act as an electron donor and accelerate the reduction of Co^{3+} to Co^{2+}. In fact, the similar phenomenon had been documented in a previous publication [57]. The phenolic moieties in biochar were found to be the electron-donating groups while quinone moieties were found to be the electron-accepting groups [58]. Moreover, the electron transfer mechanism was elucidated in highly graphitic N-doped biochar catalysts (carbonization temperature > 700 °C) [9]. Wang et al. [23] further pointed out that the different pathways were highly depended on the crystallinity of the carbocatalyst. In this case, the $MNBC_{800}$ showed a comparatively low I_D/I_G value, indicating a high graphitization degree. Consequently, the non-radical pathway was expected to be the dominant process. To confirm this hypothesis, the chemical quenching study was conducted for the NBC_{800}/PMS process. As given in Fig. S15, comparing with $MNBC_{800}$, the inhibition effect of LCP on the MET degradation by NBC_{800}/PMS process was more significant, indicating the more important role of $^1O_2$. Meanwhile, it was found that MeOH also greatly inhibited the degradation process, revealing both radical and non-radical pathways contributed to the MET degradation. Specifically, the non-radical pathway was attributed to the graphitic N in the carbon frameworks, which gave rise to the positively charged sites. Thus, the PMS could be easily adsorbed and produce electron transfer intermediates. The organic compounds were directly decomposed through electron transfer mechanism instead of by radicals [33]. Additionally, singlet oxygen could be produced through the self-decomposition of PMS (Eq. (8)) with a slow rate constant (0.2 M^{-1} s^{-1} [59,60]). Noting that, this reaction might be accelerated with assistant of MNBC catalysts.

$$Co^{2+} + HSO_5^- \rightarrow Co^{3+} + SO_4^{\bullet-} + OH^- \quad (6)$$

$$Co^{3+} + HSO_5^- \rightarrow Co^{2+} + SO_5^{\bullet-} + H^+ \quad (7)$$

$$HSO_5^- + SO_5^{2-} \rightarrow SO_4^{2-} + HSO_4^- + 1O_2 \quad (8)$$

3.4. Degradation products

Dechlorination was reported to be a main pathway of MET degradation in a photo-assisted Fenton reaction [61,62]. As manifested in Fig. 6, Cl^- was released into the reaction mixture during the degradation process, accounting to 39.2% of total Cl. This result undoubtedly confirmed the occurrence of dechlorination reaction in the degradation process. Moreover, NH_4^+ was also monitored and 1.8 mg L^{-1} NH_4^+ was detected after the degradation process, agreeing well with the previous study [63,64].

The degradation intermediates were further identified by LC-Q-TOF-MS. The corresponding spectra were given in Fig. S16. In total, 11 intermediates were detected and their possible formula were summarized in Table S2. Based on the identified degradation intermediates, a proposed degradation pathway of MET was presented in Fig. 7, involving mainly hydroxylation, dechlorination, and dealkylation reactions.

Firstly, the displacement of chloride by a hydroxyl lead to the

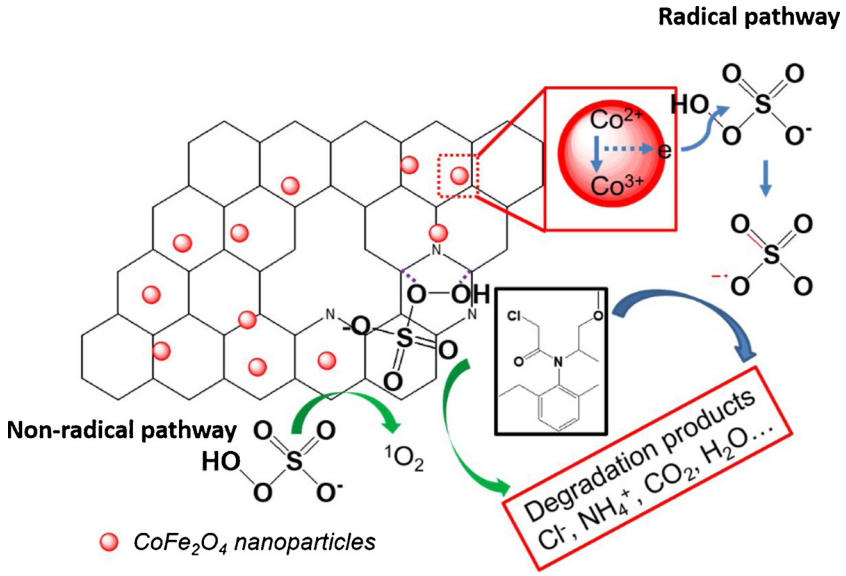

Scheme 1. Mechanism of PMS activation by $MNBC_{800}$ and MET degradation.

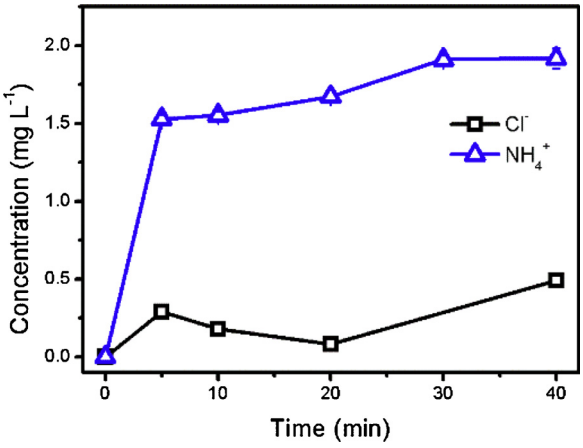

Fig. 6. Variations of the concentrations of NH_4^+ and Cl^- throughout the reaction. (Experimental conditions: [MET] = 10 mg L^{-1}, [$MNBC_{800}$] = 200 mg L^{-1}, [PMS] = 0.5 mM, pH unadjusted).

formation of 2-hydroxy-*N*-(2-ethyl-6-methylphenyl)-*N*-(2-methoxy-1-methylethyl) acetamide (P1) [65]. Then, the oxidation of *N*-Alkyl side chain occurred successively, leading to the formation of dechlorinated MET, *N*-(2-ethyl-6-methylphenyl)-*N*-(1-methoxypropan-2-yl) (P4) [66], and 2-ethyl-N-(1-hydroxypropan-2-yl)-6-methylaniline (P5) [67].

Meanwhile, demethylated MET, 2-chloro-*N*-(2-ethyl-6-methylphenyl)-*N*-(2-hydroxy-1- methylethyl) acetamide (P2) was detected in this study, which was also found in a microbial degradation process [63,68]. Then, the oxidation of the *N*-Alkyl substitute occurred, leading to the formation of 2-chloro-*N*-(2-ethyl-6-methylphenyl) acetamide (P8).

Finally, P5 and P8 were further oxidized to 2-ethyl-6-methylaniline (P10) [69] according to the loss of the *N*-alkyl substituent. Afterwards, P10 was hydroxylated to 4-hydroxy-2-ethyl-6-methyl aniline (P11) [69] and followed with the ring-opening reaction, releasing NH_4^+, CO_2, H_2O, and carboxylic acids. Noting that, this study was focused on the identification of the relatively large fragments of the produced intermediates in which the aromatic ring was intact because of their greater persistence and toxicity.

Apart from the above mentioned products, more hydroxylated

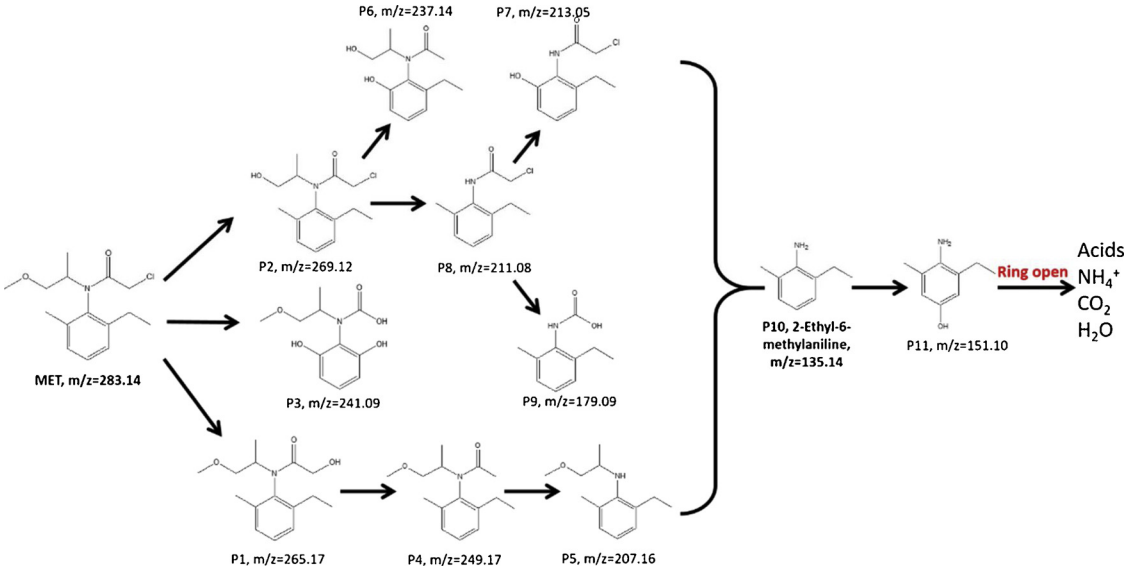

Fig. 7. Proposed degradation pathway of MET by the $MNBC_{800}$/PMS process.

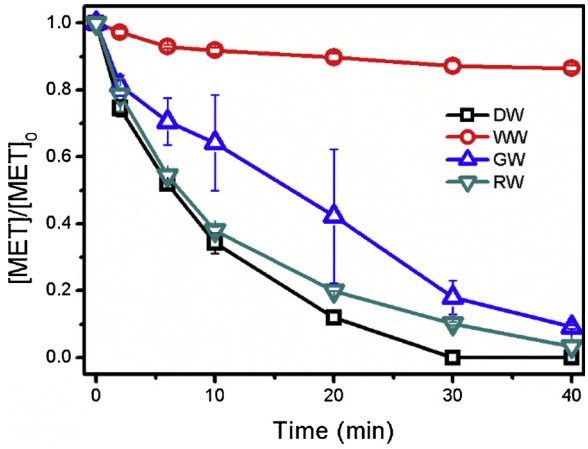

Fig. 8. Degradation of MET in deionized water (DW), wastewater (WW), groundwater (GW), and river water (RW). (Experimental conditions: [MET] = 10 mg L^{-1}, [$MNBC_{800}$] = 200 mg L^{-1}, [PMS] = 0.5 mM, pH unadjusted).

intermediates, including (2,6-dihydroxyphenyl)(1-methoxypropan-2-yl) carbamic acid (P3), *N*-(2-ethyl-6-hydroxyphenyl)-*N*-(1-hydroxypropan-2-yl) acetamide (P6) [70], 2-chloro-*N*-(2-ethyl-6-hydroxyphenyl) acetamide (P7), and (2-ethyl-6-methylphenyl) carbamic acid (P9) [31] were also identified based on the product fragments of the MS spectra (Fig. S17).

3.5. Degradation in real water

To explore the feasibility of the prepared $MNBC_{800}$ catalyst in eliminating MET from real aquatic systems, the catalytic degradation reaction was carried out in real water samples. As depicted in Fig. 8, the degradation process was unremarkably affected in RW, moderately and significantly inhibited in GW and WW, respectively. The decline of the degradation in WW was expectable because of the high concentrations of the organic/inorganic substances (Table S1) through the following reactions (Eqs. (9)–(16)). Large amounts of organic matters in WW would scavenge the reactive radical species ($k_{SO4\cdot-+DOM}$ = 6.8 × 10^3 mg $C^{-1}s^{-1}$, $k_{\cdot OH+DOM}$ = 1.4 × 10^4 mg C^{-1} s^{-1}), remarkably inhibiting the generation of radical species. Similarly, the inhibitory phenomenon in wastewater was extensively reported in other works [71,72]. The rapid degradation of MET in RW and GW implied that the applications of $MNBC_{800}$/PMS in river and groundwater remediation were possible.

$$SO_4^{-\cdot} + Cl^- \rightarrow Cl\cdot + SO_4^{2-},\ k = 3.0 \times 10^8 M^{-1}s^{-1} \quad (9)$$

$$HSO_5^- + Cl^- \rightarrow SO_4^{2-} + HOCl \quad (10)$$

$$SO_4^{-\cdot} + HCO_3^- \rightarrow HCO_3\cdot + SO_4^{2-},\ k = 2.8 - 9.1 \times 10^6 M^{-1}s^{-1} \quad (11)$$

$$SO_4^{-\cdot} + CO_3^{2-} \rightarrow CO_3^{-\cdot} + SO_4^{2-},\ k = 6.1 - 410 \times 10^6 M^{-1}s^{-1} \quad (12)$$

$$SO_4^{-\cdot} + HPO_4^{2-} \rightarrow HPO_4\cdot + SO_4^{2-},\ k = 1.2 \times 10^6 M^{-1}s^{-1} \quad (13)$$

$$Cl^- + HO\cdot \rightarrow ClHO^{-\cdot},\ k_f = (2.6 \pm 0.6) \times 10^{10} M^{-1}s^{-1};\ k_r = (3.6 \pm 0.6) \times 10^3 M^{-1}s^{-1} \quad (14)$$

$$HO\cdot + HCO_3^- \rightarrow CO_3^{2-} + H_2O,\ k = 8.5 \times 10^6 M^{-1}s^{-1} \quad (15)$$

$$HO\cdot + HPO_4^{2-} \rightarrow HPO_4^{-\cdot} + OH^-,\ k = 1.5 \times 10^5 M^{-1}s^{-1} \quad (16)$$

3.6. Toxicity evaluation

Sakkas et al. [69] claimed that the photocatalytic degradation products of MET were more toxic compared to parent compound based on the toxicity evaluation results by using Vibrio fischeri. However, in this study, the toxicity was significantly reduced after the degradation process by using green alga as a receptor. As shown in Fig. 9, fresh MET solution (400 mg L^{-1}) exhibited significant inhibition on the alga growth. Three representative samples collected at degradation time of 2 h (degradation efficiency: 20.1 ± 0.2%), 20 h (degradation efficiency: 88.3 ± 0.1%), and 30 h (complete degradation) showed lower toxicity compared with fresh MET solution, indicating the reduction of toxicity by $MNBC_{800}$/PMS process. Similarly, Mermana et al. [65] found a significant decrease in toxicity (1.7-fold reduction after 180 min of irradiation treatment) of the photocatalytic degraded MET by using alga *Pseudokirchneriella subcapitata*. Dechlorination was probably associated with the reduced toxicity since it usually resulted in the detoxification of a pesticide [69].

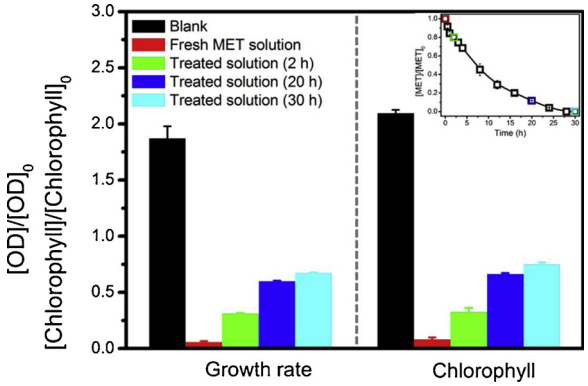

Fig. 9. Toxicity of fresh MET solution and treated MET solutions to the green alga Chlorella sp. (Experimental conditions: [MET] = 400 mg L^{-1}, [$MNBC_{800}$] = 200 mg L^{-1}, [PMS] = 0.5 mM, pH unadjusted, inset figure shows the degradation curve of MET by $MNBC_{800}$/PMS process).

Noting that, 2-ethyl-6-methylaniline, which was a typical by-product of the oxidation of MET was identified in this study (P10). This product was known for its high toxicity and thus of considerable concern. It was reported to be up to 6.3 times more acutely toxic than its parent compound [73]. However, the reduction of toxicity after the catalytic degradation process implied that this product was relatively easy to be degraded, agreeing well with previous findings. For example, Restivo et al. [62] found that the intermediate 2-ethyl-6-methylaniline could be completely removed after 30 min of catalytic ozonation treatment. Overall, the significant reduction of toxicity suggested that the developed $MNBC_{800}$/PMS process was promising for the field applications.

4. Conclusions

A series of magnetic nitrogen doped biochar (MNBC) catalysts were prepared from agricultural biomass waste (rice straw). Efficient degradation of metolachlor (MET) by MNBC catalysts coupling with peroxymonosulfate (PMS) was achieved. Additionally, the catalytic activity was highly dependent on the pyrolysis temperature. Among others, $MNBC_{800}$ catalyst performed the best catalytic activity and stability due to its highest specific surface area and graphitization degree. The degradation process was pH-dependent and favorable at neutral and weak basic conditions. Both radical and non-radical pathway contributed to the catalytic degradation while the former one played a crucial role. The herbicide was degraded mainly via hydroxylation, dechlorination, and dealkylation reactions, leading to eleven organic intermediates and inorganic substances (Cl^- and NH_4^+). More importantly, the degradation products exhibited lower toxicity than their parent compound. The low leachable metal ions, magnetically recoverable, and feasibility in different water matrices (river water and groundwater) make the prepared $MNBC_{800}$ catalyst promising for the remediation of organic pollutants from aquatic systems.

Acknowledgements

This work is financially supported by the National Natural Science Foundation of China (No. 51608274), National Science and Technology Major Project (No. 2017ZX07204001-06), the Research Foundation of Jiangsu Environmental Protection Department (No. 2017002), and the Fundamental Research Funds for the Central Universities (KYZ 201619, KJQN 201749).

Appendix A. Supplementary data

Supplementary material related to this article can be found, in the online version, at doi:https://doi.org/10.1016/j.apcatb.2019.05.014.

References

[1] X. Zuo, A Research on the Development and Utilization of the Agricultural Residues as New Sources Energy in China, Chinese Academy of Agricultural Sciences, 2015.
[2] J. Lehmann, S. Joseph, Biochar for Environmental Management, 2nd edition, (2015).
[3] M. Ahmad, A.U. Rajapaksha, J.E. Lim, M. Zhang, N. Bolan, D. Mohan, M. Vithanage, S.S. Lee, Y.S. Ok, Chemosphere 99 (2014) 19–33.
[4] P. Godlewska, H.P. Schmidt, Y.S. Ok, P. Oleszczuk, Bioresour. Technol. 246 (2017) 193–202.
[5] M. Hussain, M. Farooq, A. Nawaz, A.M. Al-Sadi, Z.M. Solaiman, S.S. Alghamdi, U. Ammara, Y.S. Ok, K.H.M. Siddique, J. Soils Sediments (2016) 1–32.
[6] F.R. Oliveira, A.K. Patel, D.P. Jaisi, S. Adhikari, H. Lu, S.K. Khanal, Bioresour. Technol. 246 (2017) 110–122.
[7] G. Fang, J. Gao, C. Liu, D.D. Dionysiou, Y. Wang, D. Zhou, Environ. Sci. Technol. 48 (2014) 1902–1910.
[8] P. Hu, M. Long, Appl. Catal. B Environ. 181 (2016) 103–117.
[9] S. Zhu, X. Huang, F. Ma, L. Wang, X. Duan, S. Wang, Environ. Sci. Technol. 52 (2018) 8649–8658.
[10] X. Duan, Z. Ao, D. Li, H. Sun, L. Zhou, A. Suvorova, M. Saunders, G. Wang, S. Wang, Carbon 103 (2016) 404–411.
[11] H.W. Liang, X.D. Zhuang, S. Bruller, X.L. Feng, K. Mullen, Nat. Commun. 5 (2014) 7.
[12] L. Chen, S. Yang, X. Zuo, Y. Huang, T. Cai, D. Ding, Chem. Eng. J. 354 (2018) 856–865.
[13] C.-D. Dong, C.-W. Chen, C.-M. Hung, Bioresour. Technol. 245 (2017) 188–195.
[14] D. Ouyang, J. Yan, L. Qian, Y. Chen, L. Han, A. Su, W. Zhang, H. Ni, M. Chen, Chemosphere 184 (2017) 609–617.
[15] D. Ding, C. Liu, Y. Ji, Q. Yang, L. Chen, C. Jiang, T. Cai, Chem. Eng. J. 308 (2017) 330–339.
[16] J. Yan, M. Lei, L. Zhu, M.N. Anjum, J. Zou, H. Tang, J. Hazard. Mater. 186 (2011) 1398–1404.
[17] G.P. Anipsitakis, D.D. Dionysiou, Environ. Sci. Technol. 38 (2004) 3705–3712.
[18] L. Chen, X. Zuo, L. Zhou, Y. Huang, S. Yang, T. Cai, D. Ding, Chem. Eng. J. 345 (2018) 364–374.
[19] L. Chen, D. Ding, C. Liu, H. Cai, Y. Qu, S. Yang, Y. Gao, T. Cai, Chem. Eng. J. 334 (2018) 273–284.
[20] Y. Wang, C.H. Zhang, M.M. Lin, Y. Ge, J. Hazard. Mater. 318 (2016) 443–451.
[21] R.A. Brown, A.K. Kercher, T.H. Nguyen, D.C. Nagle, W.P. Ball, Org. Geochem. 37 (2006) 321–333.
[22] A.C. Ferrari, D.M. Basko, Nat. Nanotechnol. 8 (2013) 235.
[23] N. Wang, W. Ma, Z. Ren, Y. Du, P. Xu, X. Han, J. Mater. Chem. A 6 (2018) 884–895.
[24] Z.-H. Sheng, L. Shao, J.-J. Chen, W.-J. Bao, F.-B. Wang, X.-H. Xia, ACS Nano 5 (2011) 4350–4358.
[25] F. Zheng, Y. Yang, Q. Chen, Nat. Commun. 5 (2014) 5261.
[26] G. Wang, S. Chen, X. Quan, H. Yu, Y. Zhang, Carbon 115 (2017) 730–739.
[27] J. Shi, Y. Wang, W. Du, Z. Hou, Carbon 99 (2016) 330–337.
[28] X. Duan, H. Sun, Y. Wang, J. Kang, S. Wang, ACS Catal. 5 (2015) 553–559.
[29] L. Lu, Q. Hao, W. Lei, X. Xia, P. Liu, D. Sun, X. Wang, X. Yang, Small 11 (2015) 5833–5843.
[30] X. Wang, Y. Qin, L. Zhu, H. Tang, Environ. Sci. Technol. 49 (2015) 6855–6864.
[31] D.R.V. Guelfi, F. Gozzi, A. Machulek Jr., I. Sirés, E. Brillas, S.C. de Oliveira, Catal. Today 313 (2018) 182–188.
[32] X. Pan, J. Chen, N. Wu, Y. Qi, X. Xu, J. Ge, X. Wang, C. Li, R. Qu, V.K. Sharma, Z. Wang, Water Res. 143 (2018) 176–187.
[33] X. Chen, W.-D. Oh, Z.-T. Hu, Y.-M. Sun, R.D. Webster, S.-Z. Li, T.-T. Lim, Appl. Catal. B Environ. 225 (2018) 243–257.
[34] H. Sun, Y. Wang, S. Liu, L. Ge, L. Wang, Z. Zhu, S. Wang, Chem. Commun. 49 (2013) 9914–9916.
[35] W.-D. Oh, G. Lisak, R.D. Webster, Y.-N. Liang, A. Veksha, A. Giannis, J.G.S. Moo, J.-W. Lim, T.-T. Lim, Appl. Catal. B Environ. 233 (2018) 120–129.
[36] P.R. Shukla, S. Wang, H. Sun, H.M. Ang, M. Tadé, Appl. Catal. B Environ. 100 (2010) 529–534.
[37] F.J. Rivas, O. Gimeno, T. Borallho, Chem. Eng. J. 192 (2012) 326–333.
[38] P. Shi, X. Dai, H. Zheng, D. Li, W. Yao, C. Hu, Chem. Eng. J. 240 (2014) 264–270.
[39] S. Pylypenko, S. Mukherjee, T.S. Olson, P. Atanassov, Electrochim. Acta 53 (2008) 7875–7883.
[40] S. Su, W. Guo, Y. Leng, C. Yi, Z. Ma, J. Hazard. Mater. 244 (2013) 736–742.
[41] Y. Ren, L. Lin, J. Ma, J. Yang, J. Feng, Z. Fan, Appl. Catal. B Environ. 165 (2015) 572–578.
[42] T. Zhang, H. Zhu, J.-P. Croué, Environ. Sci. Technol. 47 (2013) 2784–2791.
[43] K.H. Chan, W. Chu, Water Res. 43 (2009) 2513–2521.
[44] L. Chen, X. Zuo, S. Yang, T. Cai, D. Ding, Chem. Eng. J. 359 (2019) 373–384.
[45] X. Duan, H. Sun, Z. Shao, S. Wang, Appl. Catal. B Environ. 224 (2018) 973–982.
[46] R.A. Floyd, L.M. Soong, Biochem. Biophys. Res. Commun. 74 (1977) 79–84.
[47] S.V. Verstraeten, S. Lucangioli, M. Galleano, Inorganica Chim. Acta 362 (2009) 2305–2310.
[48] G.D. Mao, P.D. Thomas, M.J. Poznansky, Free Radic. Biol. Med. 16 (1994) 493–500.
[49] J.R. Harbour, S.L. Issler, M.L. Hair, J. Am. Chem. Soc. 102 (1980) 7778–7779.
[50] P. Shao, J. Tian, F. Yang, X. Duan, S. Gao, W. Shi, X. Luo, F. Cui, S. Luo, S. Wang, Adv. Funct. Mater. 28 (2018) 1705295.
[51] S. Yang, X. Qiu, P. Jin, M. Dzakpasu, X.C. Wang, Q. Zhang, L. Zhang, L. Yang, D. Ding, W. Wang, K. Wu, Chem. Eng. J. 353 (2018) 329–339.
[52] H. Sun, S. Liu, G. Zhou, H.M. Ang, M.O. Tadé, S. Wang, ACS Appl. Mater. Interfaces 4 (2012) 5466–5471.
[53] W.-D. Oh, Z. Dong, T.-T. Lim, Appl. Catal. B Environ. 194 (2016) 169–201.
[54] P.D. Hu, H.R. Su, Z.Y. Chen, C.Y. Yu, Q.L. Li, B.X. Zhou, P.J.J. Alvarez, M.C. Long, Environ. Sci. Technol. 51 (2017) 11288–11296.
[55] D. Li, X. Duan, H. Sun, J. Kang, H. Zhang, M.O. Tade, S. Wang, Carbon 115 (2017) 649–658.
[56] X. Duan, H. Sun, J. Kang, Y. Wang, S. Indrawirawan, S. Wang, ACS Catal. 5 (2015) 4629–4636.
[57] Y.X. Qin, L.Z. Zhang, T.C. An, ACS Appl. Mater. Interfaces 9 (2017) 17116–17125.
[58] L. Klüpfel, M. Keiluweit, M. Kleber, M. Sander, Environ. Sci. Technol. 48 (2014) 5601–5611.
[59] D.F. Evans, M.W. Upton, J. Chem. Soc. Dalton Trans. (1985) 1151–1153.
[60] D.L. Ball, J.O. Edwards, J. Am. Chem. Soc. 78 (1956) 1125–1129.
[61] P.L. Huston, J.J. Pignatello, Water Res. 33 (1999) 1238–1246.
[62] J. Restivo, J.J.M. Órfão, S. Armenise, E. Garcia-Bordejé, M.F.R. Pereira, J. Hazard. Mater. 239–240 (2012) 249–256.
[63] J.J. Pignatello, Y. Sun, Water Res. 29 (1995) 1837–1844.
[64] C.A. Orge, M.F.R. Pereira, J.L. Faria, Chem. Eng. J. 318 (2017) 247–253.
[65] J. Mermana, P. Sutthivaiyakit, C. Blaise, F. Gagné, S. Charnsethikul, P. Kidkhunthod, S. Sutthivaiyakit, Environ. Sci. Pollut. Res. 24 (2017) 4077–4092.
[66] A. Thiam, R. Salazar, Environ. Sci. Pollut. Res. (2018).
[67] H.-U. Blaser, H.-P. Buser, K. Coers, R. Hanreich, H.-P. Jalett, E. Jelsch, B. Pugin, H.-D. Schneider, F. Spindler, A. Wegmann, CHIMIA Int. J. Chem. 53 (1999) 275–280.
[68] D. Sanyal, G. Kulshrestha, J. Agric. Food Chem. 50 (2002) 499–505.
[69] V.A. Sakkas, I.M. Arabatzis, I.K. Konstantinou, A.D. Dimou, T.A. Albanis, P. Falaras, Appl. Catal. B Environ. 49 (2004) 195–205.
[70] C. Liu, L. Chen, D. Ding, T. Cai, Chem. Eng. J. (2019).
[71] L. Chen, T. Cai, C. Cheng, Z. Xiong, D. Ding, Chem. Eng. J. 351 (2018) 1137–1146.
[72] Y. Xiao, L. Zhang, J. Yue, R.D. Webster, T.-T. Lim, Water Res. 75 (2015) 259–269.
[73] O. Osano, W. Admiraal, H.J.C. Klamer, D. Pastor, E.A.J. Bleeker, Environ. Pollut. 119 (2002) 195–202.